

Shuang Zhai

Su Zhou¹

e-mail: suzhou@tongji.edu.cn

School of Automotive Studies,
Clean Energy Automotive Engineering Center,
Sino-German Postgraduate School,
Tongji University,
201804 Shanghai, China

Pengtao Sun

Department of Mathematical Sciences,
University of Nevada, Las Vegas,
4505 Maryland Parkway,
Las Vegas, NV 89154

Fengxiang Chen

Jigao Niu

College of Automotive Engineering,
Tongji University (Jiading Campus),
4800 Caoan Road,
Shanghai 201804, China

Modeling Study of Anode Water Flooding and Gas Purge for PEMFCs

A one-dimensional, dynamic proton exchange membrane fuel cells stack model is developed in this paper, where the transports of reactant and water (in both liquid and vapor phase) are described by partial differential equations (PDEs) in gas diffusion layers (GDLs) of both anode and cathode, and the lumped model is applied to channels and MEA. The boundary conditions needed for PDEs in GDLs are provided by the lumped model. In addition, the convection term is considered in PDEs for GDLs to describe the convection effect on hydrogen gas purge process on the anode side. As a result, the purge effect under medium current density (corresponding to ohmic polarization dominated region) can be simulated in an efficient manner by improving the mass transfer and reducing the effect of water back diffusion from cathode to anode. The presented gas purge model is validated by the experimental data obtained from our laboratory as well as other research group. The influence factors to the gas purge schedule on the anode side, such as the purge interval and purge time, are investigated as well. [DOI: 10.1115/1.4006053]

1 Introduction

Owing to their high energy efficiency, low pollution, low noise, low operating temperatures, quiet operation, fast start up and shut down, proton exchange membrane fuel cells (PEMFCs) are widely regarded as a promising technology for mobile, stationary, and portable application [1,2].

However, factors such as durability and cost still remain as the major barriers to fuel cell commercialization. There are some concurrent problems related with the two factors arising in a PEMFC power system. For example, when the PEMFC operates in a dead-end mode on the anode side, how to control the anode purge valve to achieve both high fuel efficiency and stable cell performance. It is well known that the flooding due to liquid water accumulation can significantly deteriorate fuel cell performance; impurities accumulate in the fuel cell anode will lead to fuel cell performance decrease as well. On the other hand, the fuel efficiency can be reduced if the purge interval time is too short; pressure wave transmission generated in the flow channels during the purge valve switch on and off may lead to mechanical vibrations of the membrane electrode assembly (MEA) and accelerate its damaging [3,4].

Considerable researches on the relevant topics have been done in the literature. Himanen et al. [5] reported that anode side flooding can be reduced at higher anode gas pressure due to the increased hydraulic permeation of water through the membrane. Corresponding to hydrogen pressure drops, Corbo et al. [6] showed that a slight voltage recovery due to purge intervention can be observed for those cells that are more affected by the incoming water flooding. Bussayajarn et al. [7] compared the purge effects on different cathode design (parallel slit, circular open and oblique slit). They found that the three cathodes' designs are not easy to distinguish as they all reach the same current

density level; this is because the cell performance is dominated by water accumulation rather than oxygen transportation. Fabian et al. [8] declared that purge is required to remove the overproduced water, inert impurities presented in the hydrogen, and the nitrogen diffused from the cathode to the anode. The accumulated nitrogen decreases the partial pressure of hydrogen and therefore reduces fuel cell current density. According to their experimental result, Müller et al. [9] also showed that it is necessary to make the purge schedules optimal and safe in order to lessen the water and nitrogen accumulation in the anode. Carlson et al. [10] stated that when purge fractions is lower than 0.6%, the increase of the nitrogen concentration in the anode compartment results in a lower cell voltage and hence a lower efficiency. On the other hand, when purge fraction is too high, a majority of the freshly fed hydrogen is purged out of the system without being electrochemically utilized and hence the efficiency is decreased. Furthermore, they also pointed out that a thinner membrane (<50 microns) needs higher hydrogen purge rate in order to avoid anode flooding. By controlling each cell's exhaust and providing the water management necessary, Nguyen et al. [11,12] developed a method to achieve a good performance for fuel cell stack.

Xiao et al. [13] studied two purge patterns, i.e., intermittent purge and annular purge, and concluded that the intermittent purge greatly affects fuel cell performance and thus it is not suitable for the in situ application; the annular purge process requires a higher pressure drop, and the critical pressure drop is calculated from the annular purge model. The results showed that the annular purge is appropriate for removing liquid water from the anode. Gou et al. [4] also presented a one-dimensional computational fluid dynamics model for PEMFC, and found that a long purge time is necessary to show the entire pressure drop curve, while only a part of the curve can be attained if a short purge time is adopted, along with a relatively uniform distribution of pressure swing which represents the top value of pressure variation at certain point in the channel during the purge process.

Stefanopoulou et al. [14] described a simple two-phase flow dynamic model where an anode purge sub-model was included as

¹Corresponding author.

Contributed by the Advanced Energy Systems Division of ASME for publication in the JOURNAL OF FUEL CELL SCIENCE AND TECHNOLOGY. Manuscript received November 6, 2011; final manuscript received December 7, 2011; published online April 19, 2012. Editor: Nigel M. Sammes.

well. This model precisely captured the trend of the voltage recovery after an anode purge event occurs. Based on their model presented in Refs. [15–17] and the tunable physical parameters identified by experimental data, McKay et al. discussed in detail the relationship between stack performance and anode purge. In this paper, we improve their model in the following two aspects:

- (1) The convective transport of gas, which was neglected in Refs. [14–16], is considered, especially for medium current density case.
- (2) The control strategy of gas purge schedule on the anode side is given according to the purge model and the corresponding experiment.

The objective of this paper is to extend the purge model of Refs. [14–18] from low to a medium current density level by considering both aspects listed above. The improved model shall be validated by comparing the simulated results with the experimental data shown in our recent work [19]. Furthermore, the influencing factors to the gas purge schedule on the anode side is investigated as well.

The rest of this paper is organized as follows. We describe a one-dimensional PDE model for the transports of reactant and water in GDL and a lumped model in MEA and channel in Sec. 2, introduce the formulation of polarization curve in Sec. 3, and carry out the numerical implementation and elucidation in Sec. 4.

2 Mathematical Model

2.1 Model Assumptions. To develop a transport model for the reactant and water (presenting in both liquid and vapor phase), we need to introduce the following necessary assumptions:

- Oxygen and nitrogen molecules do not cross over through the membrane [17].
- The loss current density (see Eq. (36) at below) is caused by hydrogen that permeates the membrane to the cathode side and then reacts with oxygen [20].
- There is no appreciable contact resistance against the conduction of heat, electrons, or ions [21].
- Water in both vapor and liquid phase exists in the stack.
- Ideal gas law is employed for the gaseous species.
- The internal cell structure (gas channel, GDL and MEA) is assumed to be isothermal [15].
- Gravity force is not taken into account.
- The distribution of cell voltage in the stack is uniform.
- Each individual fuel cell is divided into five parts, i.e., gas channel and GDL on both anode and cathode sides. The transports of reactant and water (in both liquid and vapor phase) are described by one-dimensional PDEs in GDLs; whereas the lumped models are applied to channels and MEA, providing the boundary conditions for the PDEs in GDLs.
- Note that the reaction in certain area on the cathode side is reduced because fewer proton is transferred from anode side to cathode side, if the interface of catalyst layer and membrane is occupied by the accumulated liquid water on the anode side. Therefore, we assume that anode and cathode have the same apparent fuel cell area, A_{app} , as defined in Eq. (38). This assumption is useful for the derivation of Eq. (37).

2.2 Capillary Transport of Liquid Water in GDL. As described in Ref. [14], in hydrophobic GDL material, the capillary pressure increases as the pore spaces in GDL are filled with liquid water, causing the water to flow through the adjacent pores where less water exist. This process creates a liquid water flow through GDL, resulting in a liquid injection into the channel. By applying the conservation law of mass to the GDL volume, the liquid water dynamics, which arises from the capillary liquid water mass flow, W_1 , and the molar evaporation rate, R_{evap} , can be defined as [15]:

$$\frac{\partial s}{\partial t} = \left(\frac{1}{\rho_1 \varepsilon A_{fc}} \right) \frac{\partial W_1}{\partial y} - \frac{R_{evap} M_V}{\rho_1} \quad (1)$$

where the mass of liquid water in GDL is expressed in terms of liquid water saturation, s , which represents the fraction of the liquid volume to the pore volume ($s = V_l/V_p$), A_{fc} is nominal fuel cell active area, ρ_1 is liquid water density, M_V is the molecular weight of water, and ε is GDL porosity. Here y represents the one-dimensional coordinate variable.

The mass flow of liquid water through GDL is a function of the gradient of capillary pressure, described by Refs. [15, 22]:

$$W_1 = - \frac{\varepsilon A_{fc} \rho_1 K K_{r1}}{\mu_1} \left(\frac{\partial p_c}{\partial S} \right) \left(\frac{\partial S}{\partial y} \right) \quad (2)$$

where p_c denotes the capillary pressure of liquid water, K is absolute permeability, μ_1 represents the viscosity of liquid water, and S denotes the reduced liquid water saturation, defined as Ref. [15]:

$$S = \begin{cases} \frac{s - s_{im}}{1 - s_{im}} & \text{for } s_{im} < s < 1 \\ 0 & \text{for } 0 \leq s \leq s_{im} \end{cases} \quad (3)$$

where s_{im} is the immobile saturation describing the critical saturation value at which the liquid water path becomes discontinuous and capillary flow is interrupted. This capillary flow interruption occurs when $s < s_{im}$. The relative permeability function of liquid water, K_{r1} , showing more available pathways for capillary flow as liquid water saturation increases, is a function of the reduced liquid water saturation, S , given by [23]:

$$K_{r1} = S^4 \quad (4)$$

Capillary pressure is the surface tension of water droplet integrated over the surface area, defined as [15]:

$$p_c = \frac{\sigma \cos \theta_c}{\sqrt{K/\varepsilon}} [1.417S - 2.120S^2 + 1.263S^3] \quad (5)$$

where σ is the surface tension between water and air, and θ_c is the contact angle of the water droplet.

Finally, the molar evaporation rate reads [16]:

$$R_{evap} = \gamma \frac{p_{sat} - p_v}{RT} \quad (6)$$

where γ is the volumetric condensation coefficient, R is ideal gas constant, T is temperature, p_{sat} denotes water vapor saturation pressure that is a function of temperature [24], and p_v is the partial pressure of water vapor. If $p_{sat} < p_v$, then $R_{evap} < 0$, which means the condensation of water. A logical constraint must be included such that if no liquid water is presented ($s = 0$) and $p_{sat} > p_v$, then water shall not be evaporated ($R_{evap} = 0$).

2.3 Gas Species Transport in GDL. The gas species transport in the porous medium, i.e., GDL, is driven by convection and diffusion. Because flow velocity plays the main role in convection coefficient, the convection spreads its influence along flow direction only, whereas the diffusion process affects the gas distribution along the gradient of concentration in all directions, due to Fick's law.

The convection effect, which is usually neglected under low current density, is considered under medium current density in this paper as an extension of [15, 16]. The convective flux can be expressed as:

$$N_{c,k} = u C_k \quad (7)$$

where $N_{c,k}$ is the convective flux of the k -th species, u is velocity of gas flow, and C_k represents molar concentration of the k -th species.

The relationship between gas velocity and pressure in the porous medium, can be described by Darcy's law as [23]:

$$\rho_g u = -k_{rg} \frac{K}{v_g} \frac{\partial p_g}{\partial y} \quad (8)$$

where ρ_g is the gas mixture density, defined as:

$$\rho_g = \frac{1}{\sum_i \frac{y_i}{\rho_i}} \quad (9)$$

here, y_i and ρ_i are the mass fraction and density of species i , respectively. k_{rg} is the relative permeability defined as the ratio of the intrinsic permeability of gas phase to the total permeability of a porous medium [23]:

$$k_{rg} = (1 - S)^4 \quad (10)$$

and v_g is the gas kinematic viscosity. The total gas pressure, p_g , can be calculated by ideal gas law in porous media [14,25]:

$$p_g = \left(\sum_i C_i \right) RT \quad (11)$$

where the subscript i represents gas species water vapor and hydrogen on the anode side and water vapor, oxygen and nitrogen on the cathode side. Thus, the convection term can be calculated through (7)–(11) as follows:

$$N_{c,k} = -KRT \frac{k_{rg}}{\rho_g v_g} C_k \sum_i \frac{\partial C_i}{\partial y} \quad (12)$$

The diffusional flux of gas species in the GDL is a function of the concentration gradient, transporting gas from the regions of high concentration to those of low concentration. The diffusional flux at both anode and cathode can be modeled as [15]:

$$N_{d,k} = -\langle D_k \rangle \frac{\partial C_k}{\partial y} \quad (13)$$

where $\langle D_k \rangle$ is the effective diffusivity of the gas constituents in the GDL, defined as [15]:

$$\langle D_k \rangle = D_k \varepsilon \left(\frac{\varepsilon - 0.11}{1 - 0.11} \right)^{0.785} (1 - s)^2 \quad (14)$$

Finally, the general temporal derivative of gas concentration, as a function of $N_{d,k} + N_{c,k}$, and R_k , forms a partial differential equation (PDE),

$$\frac{\partial C_k}{\partial t} = -\frac{\partial (N_{d,k} + N_{c,k})}{\partial y} + R_k \quad (15)$$

which leads to a transient diffusion-convection-reaction equation with respect to the gas concentration of species k , C_k .

2.4 Gas Species Transport in Gas Channel and MEA. This section presents the application of mass conservation in the channel as well as the model for the water vapor exchange between the anode and cathode through MEA.

The gas species transport in the anode channel are balanced by applying mass continuity [18]:

$$\frac{dm_{H_2,anch}}{dt} = W_{H_2,in} - W_{H_2,out} - W_{H_2,anch2GDL} \quad (16)$$

$$\frac{dm_{vapor,anch}}{dt} = W_{vapor,an,in} - W_{vapor,an,out} - W_{vapor,anch2GDL} + W_{evap,an} \quad (17)$$

$$\frac{dm_{liquid,anch}}{dt} = W_{liquid,an,in} - W_{liquid,an,out} + W_{liquid,anch2GDL} - W_{evap,an} \quad (18)$$

where the hydrogen inlet mass flow rate $W_{H_2, in}$ is defined as [15]:

$$W_{H_2,in} = k_{an,in} (p_{an,in} - p_{an,ch}) \quad (19)$$

where $k_{an,in}$ is an orifice constant found experimentally.

In calculating the total channel pressure at the anode, both the partial pressures of hydrogen and water vapor must be estimated such that:

$$p_{an,ch} = \frac{RT}{V_{an}} \left(\frac{m_{H_2,anch}}{M_{H_2}} + \frac{m_{vapor,anch}}{M_{H_2O}} \right) \quad (20)$$

Because the hydrogen supplied to the anode is dry, the water vapor/liquid mass flow rate on the anode side are assumed to be zero, i.e.,

$$W_{vapor,an,in} = 0 \quad \text{and} \quad W_{liquid,an,in} = 0 \quad (21)$$

The total mass flow rate of the outgoing gases in the anode channel, $W_{anch,out}$, existing only for a gas purge on the anode side to remove both hydrogen and water vapor/liquid, can be calculated by [15,18]:

$$W_{anch,out} = k_{an,out} v_{an,open} (p_{an,ch} - p_{anch,out}) \quad (22)$$

where $v_{an,open}$ is equal to 0 when the valve is closed and 1 when it is opened.

Thus, the outgoing hydrogen/vapor flow are given by:

$$W_{H_2,out} = \frac{1}{1 + w_{an}} W_{anch,out} \quad (23)$$

$$W_{vapor,out} = \frac{w_{an}}{1 + w_{an}} W_{anch,out} \quad (24)$$

where the humidity ratio, w_{an} , is usually defined by:

$$w_{an} = \frac{p_v M_v}{p_{H_2} M_{H_2}} \quad (25)$$

Condensation dynamics is calculated by [18]:

$$W_{evap,an} = \min \left(A_{fc} (p_{sat}(T_{st})) - p_{v,anch} \sqrt{\frac{M_v}{2\pi RT_{st}}} \cdot W_{liquid,anch2GDL} \right) \quad (26)$$

Furthermore, we define:

$$W_{liquid,an,out} = \frac{m_{liquid,anch}}{t_{purge}} \quad (27)$$

Based on Eq. (27), we can describe the quantity of liquid water that is removed by every gas purge. Thus, the lumped model description for the anode gas channel is completed.

The lumped model in anode gas channel can provide a time-dependent boundary condition for the one-dimensional PDE model in the GDL. In other words, we can calculate the diffusional flux of the one-dimensional model at the interface of GDL and the anode channel, according to the following relationship:

$$W_{k,anch2GDL} = N_{d,k} M_k \varepsilon A_{fc} n_{cell} \quad (28)$$

In addition, once we deduce the gas mass at the channel based on Eqs. (16) and (17), the species concentration can be obtained by:

$$C_k = \frac{m_k}{M_k V_{an}} \quad (29)$$

Moreover, the convective flux of the one-dimensional model at the interface of GDL and the anode channel can be deduced by plugging Eq. (29) into Eq. (12). Hence, via the diffusional and convective flux at the interface of the anode channel and GDL, the one-dimensional PDE model in the GDL on the anode side is linked up with the lumped model in the anode channel.

The hydrogen diffusional flux at the interface of MEA and GDL can be obtained by:

$$N_{H_2, GDL2MEA} = \frac{I}{2\varepsilon A_{fc} F} \quad (30)$$

where I is the total current drawn from the fuel cell stack and F is the Faraday constant. The molar flux of water vapor at the GDL-membrane boundary, $N_{vapor, anGDL2MEA}$, is influenced by the generation of water vapor at the cathode membrane surface and the flow of water vapor through the membrane, which are defined as [15]:

$$N_{vapor, anGDL2MEA} = \frac{1}{\varepsilon} N_{vapor, MEA} \quad (31)$$

$$N_{vapor, caGDL2MEA} = \frac{1}{\varepsilon} \left(N_{vapor, MEA} + \frac{I}{2A_{fc} F} \right) \quad (32)$$

The flux of water vapor through the membrane, $N_{vapor, MEA}$, accounts for the effects of both electro-osmotic drag and back-diffusion coming from cathode, given by [15,18,26]:

$$N_{vapor, MEA} = n_d \frac{I}{A_{fc} F} - \alpha_w D_w \frac{c_{vapor, ca, MEA} - c_{vapor, an, MEA}}{t_{mb}} \quad (33)$$

where n_d is the electro-osmotic drag coefficient; D_w is the membrane water vapor diffusion coefficient; and t_{mb} is the membrane thickness. α_w is an experimental parameter which corrects the possible deviations of the experimental values obtained from the literature. As they might be obsolete since their being based on older membranes [18]. The reader can refer to [15,18] for a detailed description of calculating the parameters above.

In addition, the models in the cathode gas channel are similar to those on the anode side with two exceptions: (1) the oxygen instead of hydrogen as the reactant; (2) the purging valve does not exist on the cathode channel outlet. Thus, $v_{ca, open}$ is equal to 1 during the operation.

So far, the sub-models of all parts have been developed, including both the anode and cathode side. Based on these models, we can simulate the process of water transport from the cathode to anode side and analyze the effect of anode purging operation on the stack performance.

3 Fuel Cell Voltage

A sufficiently accurate approximation for the fuel cell polarization curve may be obtained by the following equation [15]:

$$V = E - \eta - V_{ohm} \quad (34)$$

where V is the output voltage. E is the theoretical open circuit voltage, which is defined as [20]:

$$E = - \left(\frac{\Delta H - T \Delta S}{2F} \right) + \frac{RT}{2F} \ln \left(\frac{p_{H_2, an} \sqrt{p_{O_2, ca}}}{p_0^{1.5}} \right) \quad (35)$$

here p_0 is the standard pressure. ΔS and ΔH are the differences in entropy and enthalpy from standard state conditions. They are constants in this paper under the isothermal condition in Sec. 2.1.

η is the activation overvoltage which is needed to make the electrochemical reaction happen, expressed as [20]:

$$\eta = \frac{RT}{\alpha F} \ln \left(\frac{i_{app} + i_{loss}}{i_0} \right) \quad (36)$$

where α is the cathodic transfer coefficient of the oxygen reduction reaction, i_{loss} the loss current density due to hydrogen crossover, i_{app} the apparent current density that is a function of the reduced active area due to the accumulation of liquid water at the interface of GDL and channel, defined as:

$$i_{app} = \frac{I}{A_{app}} \quad (37)$$

The apparent fuel cell area, A_{app} , representing the decrease in surface area on the anode side due to the accumulation of liquid water, approximately reads [14]:

$$A_{app} = A_{fc} = \frac{2m_{liquid, anch}}{n_{cells} \rho_1 t_{wl}} \quad (38)$$

The scaling factor of 2 in Eq. (38) is used to account for the fact that one half of the surface area at the GDL-channel interface is occupied by channel ribs, which reduces the area available for the formation of a liquid water film [15].

i_0 is the exchange current density which is a function of the reactant partial pressure and temperature, expressed as [15,20]:

$$i_0 = i_0^{ref} a_c L_c \left(\frac{p_{O_2, ca}}{p_0} \right)^{K_1} \exp \left[- \frac{E_c}{RT} \left(1 - \frac{T}{T_0} \right) \right] \quad (39)$$

where i_0^{ref} is the reference exchange current density (at reference temperature and pressure, typically 25 °C and 101.325 kPa) per unit catalyst surface area, $A_{cm}^{-2}Pt$; a_c is catalyst specific area (theoretical limit for Pt catalyst is 2400 $cm^2 mg^{-1}$, but state-of-the-art catalyst has about 600-1000 $cm^2 mg^{-1}$, which is further reduced by incorporation of catalyst in the electrode structures by up to 30%). L_c is catalyst loading (state-of-the-art electrodes have 0.3–0.5 $mgPt cm^{-2}$, lower loadings are possible but would result in lower cell voltages). It is difficult to measure i_0^{ref} , a_c and L_c in practice; thus, we define $K_2 = i_0^{ref} a_c L_c$ as a tunable parameters; K_1 is the pressure coefficient (0.5 to 1); E_c is the activation energy for oxygen reduction on Pt, and T_0 is the reference temperature.

The ohmic voltage loss, V_{ohm} , can be calculated by:

$$V_{ohm} = IR = \frac{I \delta_{MEA}}{\kappa_{MEA}} \quad (40)$$

where δ_{MEA} is MEA thickness and κ_{MEA} is proton conductivity which can be defined as [1]:

$$\kappa_{MEA} = (0.5139\lambda - 0.326) \exp \left[1268 \left(\frac{1}{303} - \frac{1}{T} \right) \right] \quad (41)$$

Note that our operation is performed at low and medium current density. The concentration voltage loss due to a mass transport limitation at high current density is negligible [15]. Future work will include concentration voltage loss when this model is extended to the case of very high current density.

4 Numerical Implementation and Elucidation

The main objective of this section is to verify the feasibility and effectiveness of the integrated model of PEMFC described in Sec. 2 and fuel cell voltage model presented in Sec. 3. Based on the experimental data given by our laboratory, we validate that our purge model is basically correct, where the corresponding

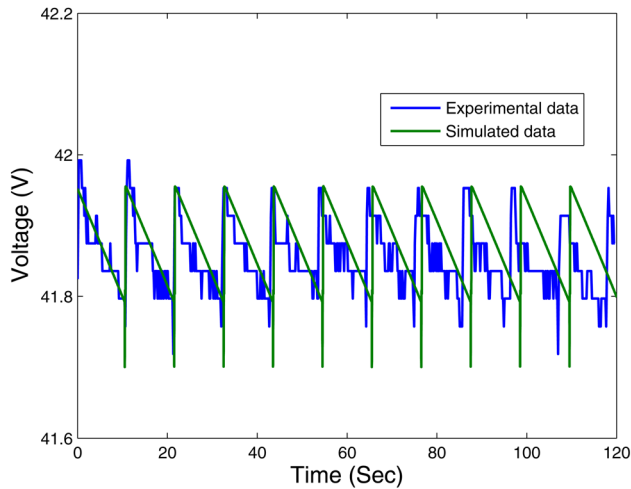


Fig. 1 Comparison of the simulated and experimental data during purge events with $i = 0.333 \text{ A/cm}^2$

tunable parameter values of α , K_1 and K_2 are adopted as 0.344, 0.0053 and 1.098, respectively. The difference of the model with and without convection term is analyzed, elucidating the high purge efficiency of our model. In addition, the control strategy of gas purge schedule on the anode side is demonstrated as well.

4.1 Model Validation and Discussion. The experimental data presented in this paper is obtained from a Horizon 1000 W fuel cell stack with an air-cooling system [27]. The stack consists of 72 individual cells, being equipped with a 54 cm^2 membrane for each cell. A dead-end mode with flush function is adopted for this hydrogen-feed fuel cell stack. Note that the cathode side of this stack is open. Thus the air supplied by the forced convection has dual function by serving as coolant as well as an oxidant. For simplicity, we assume that the fans can provide enough air to maintain the constant temperature and sufficient reactant for the stack. In addition, it is assumed that no severe “flooding” phenomenon occurs on the cathode side compared with anode operated by dead end mode.

In order to verify the model effectiveness under medium current density, the stack is operated from 0 A/cm^2 to 0.463 A/cm^2 with 0.037 A/cm^2 as the step size (the maximum current operated in this stack is 30A, corresponding to the largest current density of 0.556 A/cm^2). For simplicity, we only take the fluctuant voltages under the current densities of 0.333 A/cm^2 and 0.463 A/cm^2 as samples. The purge events are scheduled to occur after 11s for a purge time of 0.15s.

As shown in Fig. 1, the simulated results basically fit the experimental data except that more coarseness is seen. It is interesting to find that the voltage decreases with the time (about 0.2 V decrease in 11s) before the next purge event happens. When the next purge starts, the voltage quickly recovers back to the previous value (about 0.2 V increase in 0.15 s). Hence, we can conclude that the purge event can help the stack voltage recovery by removing the liquid water from the anode channel and GDL. It is even more significant under medium current density. Note that the voltage drop in an experimental stack is not totally caused by the anode but also the cathode. The water transports from the cathode to the anode through the membrane, because of pressure being reduced in the anode during the purge.

Figure 2 displays the comparison of the simulated and experimental data during purge events under the current density of 0.463 A/cm^2 . It can be seen that the simulated data fits well the experimental data. However, similar with Fig. 1, the simulated results are larger than the experimental data during two purge events, the possible reason should be the accumulation of liquid water in the anode side is more complex and may not be a simply

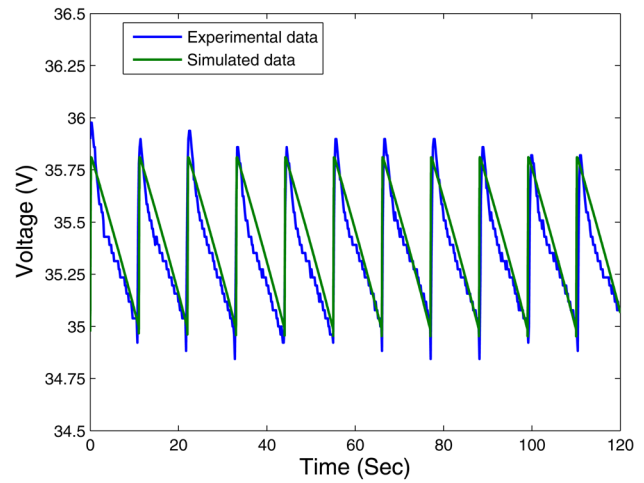


Fig. 2 Comparison of the simulated and experimental data during purge events with $i = 0.463 \text{ A/cm}^2$

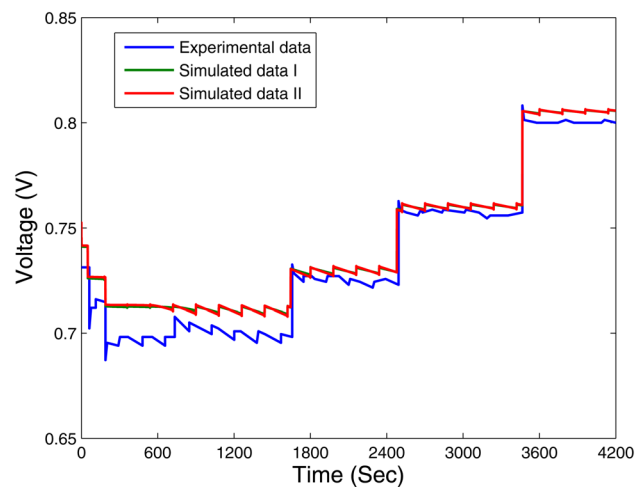


Fig. 3 Comparison of the simulated and experimental data presented in Ref. [15]

linear relationship with time as shown by the simulated results. Figure 2 shows that the fluctuation of voltage is around 1V, which is five times larger than that of 0.333 A/cm^2 . Thus, we conclude that a medium operating current density may result in a severe flooding phenomenon, and then a more positive effect on the stack performance benefited from the gas purge on the anode side.

Furthermore, we also compare the simulated results with other experimental data presented in the literature. The resulting model prediction is displayed in Fig. 3 and compared with the actual cell voltage measured at five different load levels [15]. The corresponding current density change is shown in Fig. 4. The simulated data I is obtained from the transport model including the convection term and diffusion term; whereas the simulated data II is from the transport model including the diffusion term only. As shown in Fig. 3, the simulated results fit the measured results under most of the load levels. The mismatch occurring at the first and second stage may due to the different initial conditions. In addition, we find that there is a slight difference between the simulated data I and II, which means that the convection term has little impact on the cell voltage under low current density. The further exploration will be presented in Sec. 4.2.

Thus, the purge model is validated against different measured data from low to medium current density. In next section, an elaborative analysis will be given based on this validated model.

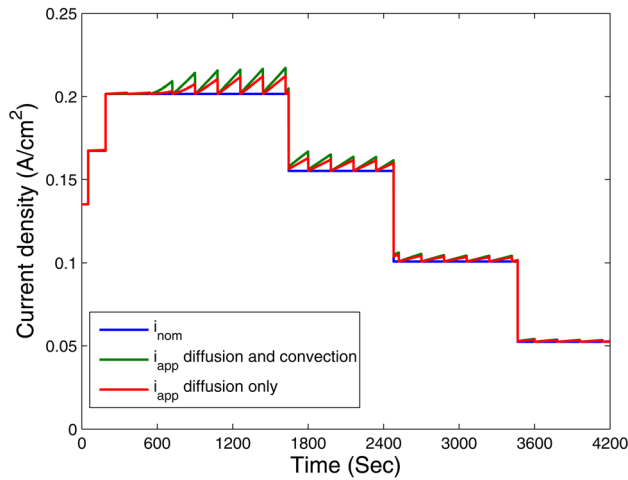


Fig. 4 Comparison of apparent current densities of the models with and without convection term

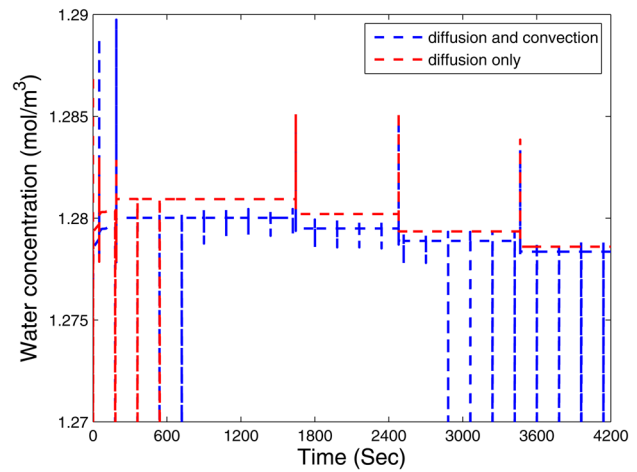


Fig. 6 Comparison of water concentrations of the models with and without convection term

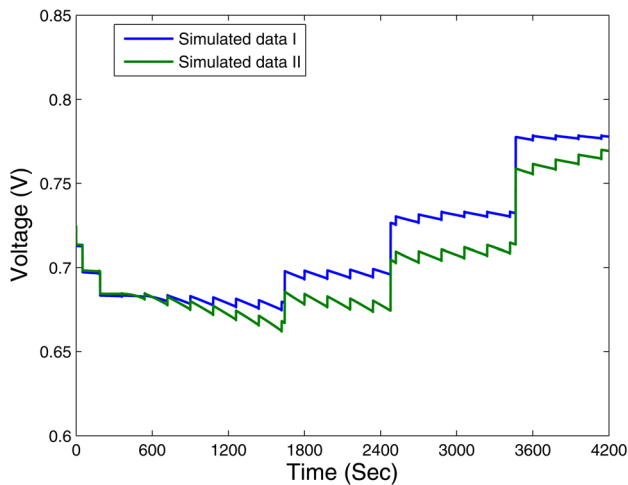


Fig. 5 Comparison of voltages of the models with and without convection term

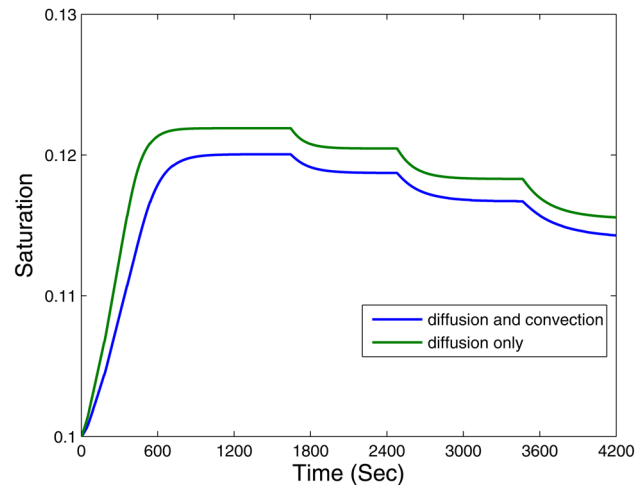


Fig. 7 Comparison of anode liquid saturations of the models with and without convection term

4.2 Investigation of the Convection Effect. By comparing Fig. 4 with Fig. 3, we find that the model with the convection term presents the smaller apparent current density in contrast to the model without convection term during the purge cycles on the anode side.

In order to further explore the effect of the convection term, we increase the load levels up to 1.5 times bigger than the ones shown in Fig. 4 in order to see how the voltage and apparent current density change. Figure 5 displays the voltages of the models with and without the convection effect. It shows that the difference between two cases is more pronounced than that shown in Fig. 3. Note that if we only consider the diffusion effect, the voltage decreases with time. However, the voltage can be maintained at the mean value if we further consider the convection effect. One explanation for such difference is that the convection effect on the anode side can reduce the effect of water back diffusion from cathode to anode and remove the liquid water from the GDL quickly due to the velocity of gas flow existing in convection term.

To prove this argument, we plot the corresponding water concentration and saturation in GDL on the anode side in Fig. 6 and Fig. 7, respectively. As shown in Fig. 6, the water concentration obtained from the model with the convection term is lower than that of the model without the convection term, especially under medium current density. Low water concentration means less liq-

uid water are produced. In addition, due to the convection effect, the velocity of gas flow can blow off the accumulated liquid water from the GDL (see Fig. 7).

Furthermore, we also present the corresponding apparent current density in Fig. 8, where the apparent current density obtained from the model without convection term demonstrates the significant change at each load level. During the third and fourth stage, the apparent current density increases with time due to the more accumulation of liquid water under medium current density. Note that a higher apparent current density is induced by a reduced active area and thus results in a higher voltage loss. It is interesting to find that the model with the convection term can keep the apparent current density decreasing with the help of a constant purge cycle. However, the model without the convection term can only reduce the apparent current density at the fifth stage, because little water is driven by back diffusion from the cathode side. Hence, many interesting simulation phenomena can be explained by the existence of convection term.

Thus, based on the improved model with the convection term being included, we can simulate the voltage fluctuation due to the purge effect from low current density to medium current density. In the following section, the gas purge schedule on the anode side will be investigated.

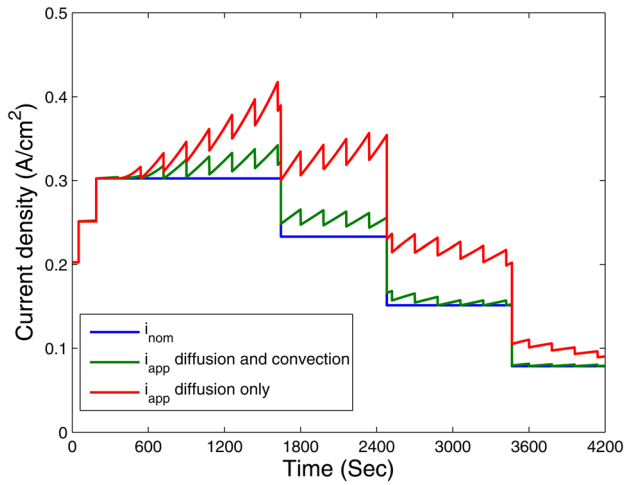


Fig. 8 Comparison of apparent current densities of the models with and without convection term (load level is up to 1.5 times bigger than that shown in Fig. 4)

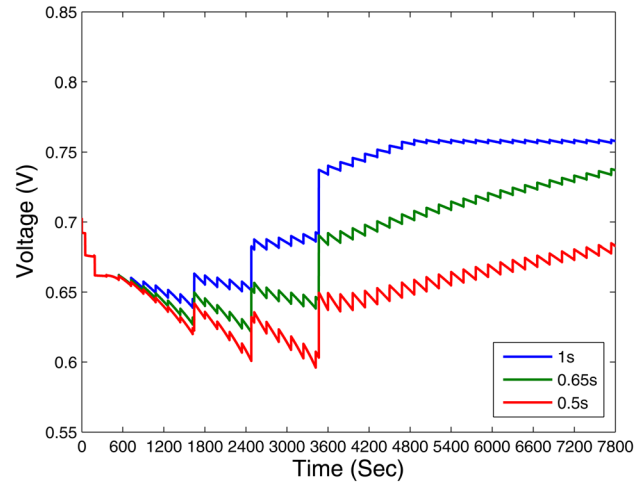


Fig. 11 Comparison of voltage's evolutions under different purge time

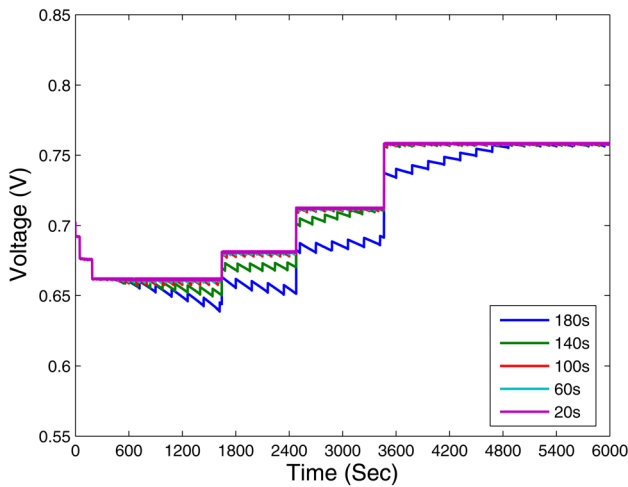


Fig. 9 Comparison of voltage's evolutions under different purge interval

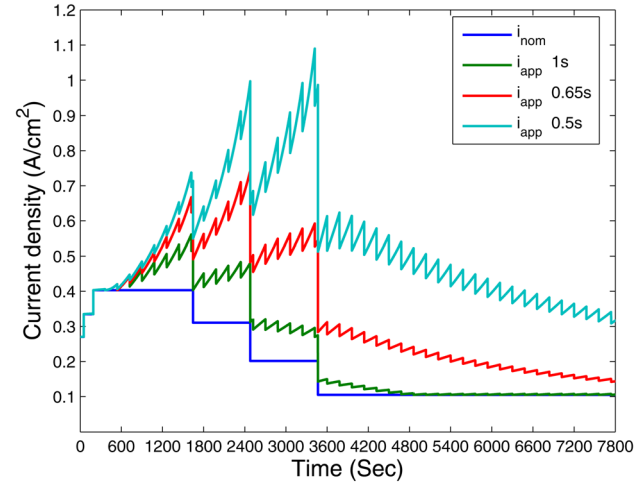


Fig. 12 Comparison of apparent current density's evolutions under different purge time

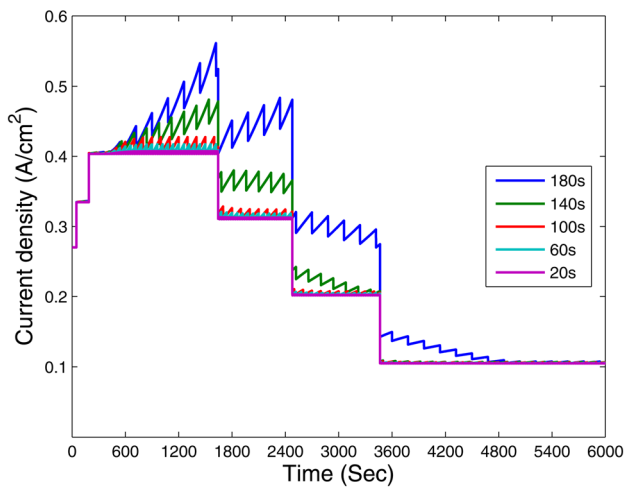


Fig. 10 Comparison of apparent current density's evolutions under different purge interval

4.3 Investigation of the Gas Purge Schedule on the Anode Side. This section discusses the effect of different purge interval and purge time on the output cell voltage. Firstly, we adopt five purge intervals, 180 s, 140 s, 100 s, 60 s and 20 s, with purge time of 1 s. As shown in Fig. 9, we can see that all of purge intervals present the same voltage during the first and the second stage for the shorter operation time. However, from the third stage, case 1 which uses 180 s as the purge interval shows serious performance degeneration. This deterioration continues to the fourth stage and stops at the fifth stage, where less liquid water is produced and the purge effect can remove this water rapidly. Note that at the last stage, the recovery rate is accelerated due to the smallest current density (see Fig. 10) and the least liquid water is produced. However, in case 2 whose purge interval is 140 s, the degree of the deterioration is alleviated in contrast to case 1. It is noteworthy that in case 3, 4, and 5, there is almost no performance degeneration due to the shorter purge interval keeping no liquid water accumulating and then no flooding phenomenon happening. But in practice, we consider not only the stack performance but also the power system efficiency. Hence, there is a compromise between them which we need to consider in order to guide our practical operation. Figure 10 displays the corresponding apparent current density which mirrors the change of voltage.

Table 1 Physical parameters and properties

Quantity	Value	Reference
Hydrogen diffusion coefficient, D_{H_2}	$1.14 \times 10^{-4} \text{ m}^2/\text{s}$	[13]
Oxygen diffusion coefficient, D_{O_2}	$3.03 \times 10^{-5} \text{ m}^2/\text{s}$	[14]
Water diffusion coefficient, D_{H_2O}	$3.55 \times 10^{-5} \text{ m}^2/\text{s}$	[18]
Activation energy, E_c	$6.6 \times 10^4 \text{ J/mol}$	[15]
Enthalpy difference, H	-228740 J/mol	[16]
Loss current density, i_{loss}	$9 \times 10^{-4} \text{ A/cm}^2$	
Absolute permeability, K	$2.55 \times 10^{-13} \text{ m}^2$	[12]
Hydrogen molecular weight, M_{H_2}	$2 \times 10^{-3} \text{ kg/mol}$	
Oxygen molecular weight, M_{O_2}	$3.2 \times 10^{-2} \text{ kg/mol}$	
Nitrogen molecular weight, M_{N_2}	$2.8 \times 10^{-2} \text{ kg/mol}$	
Water molecular weight, M_{H_2O}	$1.8 \times 10^{-2} \text{ kg/mol}$	
Standard state pressure, p_0	1 atm	
Entropy difference, S	$-44.43 \text{ J/(mol} \cdot \text{K)}$	[13]
Standard state temperature, T_0	298.15 K	
Volumetric condensation coefficient, γ	900 s^{-1}	[14]

Figure 11 presents the comparison of the voltage evolution under different purge time with the same purge interval of 180 s. It indicates that when the purge time is set as 1s, the voltage can be recovered by the purge effect. When time is 4800 s, the voltage can reach the steady state. However, when purge time are set as 0.65 s or 0.5 s, the cell performance deteriorates seriously, and the cell voltage still increases even at time = 7800 s. Figure 12 shows the change of current density which corresponds to the voltage change shown in Fig. 11. As shown in Fig. 12, the current density evolution is quite the reverse of voltage evolution. Note that some purge intervals and time in this study are used for revealing their influence on fuel cell performance under extreme conditions, which may be not suitable for practical application.

5 Conclusion and Future Work

Based on what we learned from the presented model at above, we make the conclusions in terms of the following two aspects:

- (1) The convection term can improve the mass transfer and reduce the effect of water back diffusion from cathode to anode. With the help of this mechanism, we extend the model applicability of [14] from low current density to medium current density.
- (2) Based on the purge model, the purge schedule is investigated on the anode side by comparing the effect of different purge interval and purge time on the cell voltage. The conclusion is that a shorter purge intervals and a longer purge time can result in a slighter fluctuation of the stack voltage, especially under a medium current density. We will adopt a trade-off strategy for maintaining the voltage level and improving fuel efficiency in the future work.

Acknowledgment

This work is supported by 111 Project (Grant No. B08019), Shanghai Leading Academic Discipline (Grant No. B303), the Doctoral Fund of the Ministry of Education of China (Grant No. 20090072120025), National Natural Science Foundation of China (Grant No. 61104077) and (Grant No. 11101311), and the Fundamental Research Funds for the Central Universities. Pengtao Sun is also supported in part by NSF Grant No. DMS-0913757.

Nomenclature

- A = area (m^2)
 c = molar concentration (mol/m^3)
 D = gas diffusion coefficient (m^2/s)
 E = theoretical open circuit voltage (V)
 F = Faraday's constant (96487 C/mol)

- H = enthalpy (J/mol)
 i = current density (A/cm^2)
 I = current (A)
 k = relative permeability of gas phase
 K = absolute permeability (m^2)
 m = mass (kg)
 M = molecular weight (kg/mol)
 n = number of cells in stack
 N = molar flux ($\text{mol}/(\text{m}^2 \cdot \text{s})$)
 p = pressure (Pa)
 R = gas constant ($8.314 \text{ J}/(\text{mol} \cdot \text{K})$) or reaction rate ($\text{mol}/(\text{m}^3 \cdot \text{s})$)
 s = the fraction of liquid water volume to the pore volume
 S = the reduced liquid water saturation or entropy ($\text{J}/(\text{mol} \cdot \text{K})$)
 T = temperature (K)
 u = velocity (m/s)
 V = volume or Voltage (m^3 or V)
 W = mass flow rate (kg/s)

Greek Letters

- ε = porosity
 ρ = density (kg/m^3)
 σ = ionic/electrical conductivity (S/m)
 θ = contact angle ($^\circ$)
 μ = viscosity ($\text{kg}/\text{m} \cdot \text{s}$)

Subscripts

- an = anode
 anch = anode flow channel
 anch2GDL = species change between the channel and GDL on the anode side
 app = apparent
 c = capillary or convection
 ca = cathode
 cach2GDL = species change between the channel and GDL on the cathode side
 ch = channel
 d = diffusion
 evap = evaporation
 fc = fuel cell
 im = immobile saturation
 in = anode/cathode inlet
 k = the k-th species
 l = liquid
 nom = nominal
 out = anode/cathode outlet
 v = vapor

References

- [1] Wang, C. Y., 2004, "Fundamental Models for Fuel Cell Engineering," *Chem. Rev.*, **104**, pp. 4247–4766.
- [2] Zhai, S., Zhou, S., Sun, P. T., Chen, F. X., Sundmacher, K., 2012, "Advanced Study of Non-Uniform Cell Voltage Distribution for a PEMFC Stack," *J. Fuel Cell Sci. Technol.*, **9**, pp. 011014.
- [3] Mokmeli, A., and Asghari, S., 2010, "An Investigation Into the Effect of Anode Purging on the Fuel Cell Performance," *Int. J. Hydrogen Energy*, **35**, pp. 9276–9282.
- [4] Gou, J., Pei, P. C., Wang, Y., 2006, "The Dynamic Behavior of Pressure During Purge Process in the Anode of a PEM Fuel Cell," *J. Power Sources*, **162**, pp. 1104–1114.
- [5] Himanen, O., Hottinen, T., and Tuurala, S., 2007, "Operation of a Planar Free-Breathing PEMFC in a Dead-End Mode," *Electrochem. Commun.*, **9**, pp. 891–894.
- [6] Corbo, P., Migliardini, F., and Veneri, O., 2009, "Dynamic Behaviour of Hydrogen Fuel Cells for Automotive Application," *Renewable Energy*, **34**, pp. 1955–1961.
- [7] Bussayajarn, N., Ming, H., Hoong, K. K., Stephen, W. Y. M., Hwa, C. S., 2009, "Planar Air Breathing PEMFC with Self-Humidifying MEA and Open Cathode Geometry Design for Portable Applications," *Int. J. Hydrogen Energy*, **34**, pp. 7761–7767.
- [8] Fabian, T., Posner, J. D., O'Hayre, R., Cha, S. W., Eaton, J. K., Prinz, F. B., Santiago, J. G., 2006, "The Role of Ambient Conditions on the Performance of a Planar, Air-Breathing Hydrogen PEM Fuel Cell," *J. Power Sources*, **161**, pp. 168–182.

- [9] Müller, E. A., Kolb, F., Guzzella, L., Stefanopoulou, A. G., McKay, D. A., 2010, "Correlating Nitrogen Accumulation With Temporal Fuel Cell Performance," *J. Fuel Cell Science and Technology*, **7**(2), pp. 021013-1–021013-11.
- [10] Carlson, E. J., Kopf, P., and Sinha, J., Sriramulu, S., Yang, Y., "Cost Analysis of PEM Fuel Cell Systems for Transportation," www.nrel.gov/hydrogen/pdfs/39104.pdf
- [11] Nguyen, T. V., and Knobbe, M. W., 2003, "A Liquid Water Management Strategy for PEM Fuel Cell Stacks," *J. Power Sources*, **114**, pp. 70–79.
- [12] Knobbe, M. W., He, W., Chong, P. Y., and Nguyen, T. V., 2004, "Active Gas Management for PEM Fuel Cell Stacks," *J. Power Sources*, **138**, pp. 94–100.
- [13] Xiao, Y., Ming, P. W., Hou, M., Yi, B. L., Shao, Z. G., 2009, "The Critical Pressure Drop for the Purge Process in the Anode of a Fuel Cell," *J. Power Sources*, **188**, pp. 163–169.
- [14] McKay, D. A., Ott, W. T., and Stefanopoulou, A., 2005, Proceedings of the 2005 ASME International Mechanical Engineering Congress Exposition, Report No. IMECE 2005-81484.
- [15] McKay, D. A., Siegel, J. B., Ott, W., Stefanopoulou, A. G., "Parameterization and Prediction of Temporal Fuel Cell Voltage Behavior During Flooding and Drying Conditions," *J. Power Sources*, **178**, pp. 207–222.
- [16] McKay, D. A., 2008, "Stack Level Modeling and Validation of Low Temperature Fuel Cells and Systems for Active Water Management," Ph.D. thesis, University of Michigan, Ann Arbor, MI.
- [17] Siegel, J. B., McKay, D. A., Stefanopoulou, A. G., 2008, American Control Conference, Seattle, WA, pp. 2573–2578.
- [18] del Real, A. J., Arce, A., and Bordons, C., 2007, "Development and Experimental Validation of a PEM Fuel Cell Dynamic Model," *J. Power Sources*, **173**, pp. 310–324.
- [19] Zhai, S., Zhou, S., Sun, P. T., Chen, F. X., Niu, J. G., Ding, M. C., "Experimental Investigation of Gas Purge and Voltage Undershoot for an Air-Breathing PEMFC," Proceedings of ASME 2011 5th International Conference on Energy Sustainability & 9th Fuel Cell Science, Engineering and Technology Conference ESFuelCell2011-54712.
- [20] Barbir, F., 2005, *PEM Fuel Cells: Theory and Practice*, Elsevier, New York.
- [21] Chenga, C. H., and Linb, H. H., 2009, "Numerical Analysis of Effects of Flow Channel Size on Reactant Transport in a Proton Exchange Membrane Fuel Cell Stack," *J. Power Sources*, **194**, pp. 349–359.
- [22] Nam, J. H., and Kaviany, M., 2003, "Effective Diffusivity and Water-Saturation Distribution in Single- and Two-Layer PEMFC Diffusion Medium," *Int. J. Heat Mass Transfer*, **46**, pp. 4595–4611.
- [23] Wang, Y., Basu, S., and Wang, C. Y., 2008, "Modeling Two-Phase Flow in PEM Fuel Cell Channels," *J. Power Sources*, **179**, pp. 603–617.
- [24] Zhai, S., Sun, P. T., Cheng, F. X., Zhou, S., Zhang, C. S., 2010, "Collaborative Simulation for Dynamical PEMFC Power Systems," *Int. J. Hydrogen Energy*, **35**(16), pp. 8772–8782.
- [25] Požár, N., 2008, "Porous Medium Equation," <http://www.math.ucla.edu/~npozar/doc/Porous%20medium%20equation.pdf>.
- [26] Springer, Zawodzinski, T., and Gottesfeld, S., 1991, "Polymer Electrolyte Fuel Cell Model," *J. Electrochemical Soc.*, **138**, pp. 2334–2342.
- [27] <http://www.horizonfuelcell.com>.